Journal Name

ARTICLE

Towards large scale preparation of graphene in molten salts and its use in the fabrication of highly toughened alumina ceramics

Received 00th January 20xx,
Accepted 00th January 20xx

DOI: 10.1039/x0xx00000x

www.rsc.org/

Ali Reza Kamali*, John Feighan and Derek J.Fray

Highly crystalline graphene nanosheets were reproducibly generated by the electrochemical exfoliation of graphite electrodes in molten LiCl containing protons. The graphene product has been successfully applied in several applications. This paper discusses the effect of molten salt produced graphene on the microstructure and mechanical properties of alumina articles produced by slip casting and pressureless sintering, wich is one of the most convenient methods used for the commercial production of alumina ceramics. Apart from graphene, graphite powder and multi-walled carbon nanotubes (CNTs) were also used in the preparation for comparison. The strengthening effect of graphene was realized by the microstructural refinement and by influencing the formation of alumina nanorods during sintering of α-Al_2O_3 articles. The fracture toughness of the sintered alumina articles increased to an impressive value of 6.98 MPa $m^{1/2}$ by adding 0.5wt% graphene nanosheets. It was attributed to the unique microstructure obtained comprising of micrometer sized alumina grains separated by alumina nanorods.

Introduction

During the last twenty years, molten alkali-metal halide salts have provided interesting opportunities for the production of high value materials including metals such as Ti,[1] W,[2] Zr[3] and U,[4] intermetallics such as NiTi,[5] ceramics such as $LaAlO_3$[6] and $LiNbO_3$[7] as well as new carbon materials such as carbon nanotubes,[8] nanodiamonds[9] and graphene.[10,11] Graphene has been the subject of much research, and a byword for interesting new materials and technologies since its first isolation in 2004. Most of this interest has been based on graphene's remarkable physical, chemical and mechanical properties which make graphene an ideal material for many applications including energy storage devices[12-15] as well as high performance metal-, polymer- and ceramic- based structural composites.[16-18]

However, as it has also been pointed out by Raccichini et al.,[19] the most ambitious challenge facing the widespread application of graphene is the capability of the large-scale production of high quality graphene. It is first because the high current price of quality graphene makes it uneconomic for many applications. Furthermore, most of the applications cannot be appropriately evaluated due to the lack of availability of sufficient quantity of quality graphene which is in turn due to the nonscalability of the current production methods.

In fact, most of the methods developed for the preparation of graphene, including modified Hummers method followed by reduction processes,[20] liquid phase exfoliation of graphite[21] and chemical vapour deposition techniques[22] suffer from one or more disadvantages such as the low quality of graphene product, a low rate of production, and the use of hazardous organic solvents.

It has recently been reported that graphite can be electrochemically exfoliated in molten salts to graphene nanosheets[10,11]. This process provides a unique opportunity for large-scale fabrication of high quality graphene, and thus allows many applications to be explored. This paper reports the molten salt generation of graphene and its effect on microstructure and mechanical performance of alumina ceramics prepared by slip casting and pressureless sintering which is a well known commercial method for manufacturing inexpensive ceramic articles.

Aluminium oxide (Al_2O_3) is a very important ceramic material due to its excellent combination of properties such as high melting point, hardness, strength, stiffness, wear resistance as well as chemical inertness. These properties allow alumina to be widely used in many applications, including sealing rings, high temperature electrical insulators, sheaths for high voltage lamps, refractory materials and milling media.[23,24] Moreover, alumina ceramics possess high biocompatibility and hence have been used in reconstruction of dental crowns,[25] jaws[26] and hip joints.[27] Although more than 3.5 millions alumina implants have been implemented worldwide since 1990,[27] there have also been reports on the fracture of alumina implants, since the relatively low intrinsic fracture toughness of alumina (3-5 MPa $m^{1/2}$ [28,29]). Consequently, yttria-stabilised zirconia (YSZ) has been considered as alternative to alumina as structural applications due to its higher fracture toughness brought about by a phase transformation toughening

Department of Materials Science and Metallurgy, University of Cambridge, 27 Charles Babbage Road, Cambridge CB3 0FS, UK E-mail: ark42@cam.ac.uk.

mechanism, enhancing its resistance to the crack propagation[27]. YSZ ceramics, however, suffer from low temperature degradation which largely limits its long-term practical applications.[27,30] As the result, toughening of alumina ceramics has been subject to a large number of studies, most of which have mainly been based on the incorporation of a toughening agent. In this regard, various agents and fabrication techniques have been used leading to the increase of the fracture toughness of alumina composite products. For example, a fracture toughness of 5.4, 4.8 and 5.0 MPa $m^{1/2}$ were achieved in alumina composites containing 5wt% glass phase,[31] 13 vol%Zr+Ag[32] and 13 vol. %Ni[33], respectively, using cold isostatic pressing and pressureless sintering. Hot-pressing method led to the fabrication of alumina composites containing 20 wt %YSZ[34]and 20 vol%Fe[35] with a fracture toughness of 6.8MPam$^{1/2}$ and 6.6-10.2 MPa $m^{1/2}$, respectively.

Recently, graphene has been investigated as the toughening agent in alumina ceramics. The alumina-graphene ceramics were prepared by means of spark plasma sintering, and exhibited fracture toughness values in the range of 3.5 - 5.21 MPa $m^{1/2}$. [36-38] The graphene used in these investigations were prepared by modified Hummers method followed by hydrazine reduction,[36] thermal exfoliation of intercalated graphite,[37] and liquid phase exfoliation of graphite.[38] Apart from limitations associated with the preparation of the graphene material used in these investigations, the fabrication methods employed to prepare the ceramic materials, i.e. hot pressing and spark plasma sintering processes, are costly, and involve expensive equipment. Therefore, more economical methods for the preparation of both graphene and alumina-graphene ceramics are required in order to explore the future potential of graphene in the alumina ceramic industry. It is also worthy to add that graphene materials produced by different techniques exhibit different properties. To address these, this paper investigates the effect of molten-salt produced graphene nanosheets on the microstructure and mechanical properties of alumina ceramics fabricated by means of slip casting and pressureless sintering.

Experimental

Materials

Three different carbon materials were selected for the various investigations, and these are: synthetic graphite powder (Sigma-Aldrich); commercial multiwalled carbon nanotubes (Thomas Swan, UK) produced by a gas phase process, and graphene nanosheets. The graphene nanosheets were prepared via an electrochemical method based on the intercalation of hydrogen atoms dissolved in molten LiCl into a polarized graphite (Goodfellow 809-013-12, diameter 1.3 cm, length 10 cm, purity 99.997%) allowing graphene layers to be created. The effect of these carbon materials on the microstructure and properties of alumina ceramics was investigated.

Preparation of alumina ceramics

In order to prepare the alumina ceramics, carbon materials were added to deionised water and dispersed using ultrasonication for 30 minutes. Then, sufficient amount of alumina powder (Showadenko chemicals, AL-160SG3, 99.9% purity) was added to create a slip of the desired amount of carbon, followed by a further 30 minutes of ultrasonication. The resulting slurry was ball milled at 90 rpm using a mix of 13 mm and 20 mm diameter alumina balls for 12 hours, with the powder-to-ball weight ratio of 1:5. Then, small additions of deionised water and dispersant (dispex, polyacrylate acid BASF Chemicals, AA4140, Germany) were made, in order to decrease the slurry's viscosity enhancing its cast ability, followed by a further 30 minutes of ball milling.

It should be noted that the amounts of alumina and water used depended on the amount of the carbon in the ceramic. For each sample, alumina powder was added to give a slip of the desired amount of carbon. The quantity of water was chosen to give a roughly 2:1 alumina to water weight ratio. It should also be mentioned that the pure alumina sample was also fabricated using the same processing route for comparison purposes.

The green cast bodies were then prepared using slip casting. For this, the slip was poured into plaster of Paris moulds forming rectangular specimens on loss of the water (see Fig.7). The casts were sintered in a resistant furnace under Ar protective atmosphere. For this, the temperature was raised from the room temperature to 1650° C with a heating rate of 5 ^{o} C min^{-1}, and kept at the maximum temperature for four hours.

Characterisation

The density measurements were performed via the Archimedes method. The X-ray diffraction measurements were performed on a Bruker D8 diffractometer equipped with position sensitive detector (LynxEye) and graphite 2nd beam monochromator using Cu K_{α} radiation (λ = 1.54 Å). The flexural strength was examined by three-point bending test using a Hounsfield 5kN tester with a cross-head speed of 1 mm min^{-1}. Flexural strength σ was calculated using[39]

$$\sigma = \frac{3PL}{2bh^2} \qquad (1)$$

where P is the load at the fracture point, L is the span length, b is the sample breadth, and h is the sample thickness. Hardness and indentation fracture toughness were found using Vickers indentation method. The values were measured from polished cross sections using the standard Vickers indentation procedure with a 50N load and 12 s dwell (Mitutoyo HM 100, Japan).The fracture toughness was determined by measuring the radial crack lengths produced by the Vickers indentations. Several measurements were conducted at different locations on the samples. Calculation of the fracture toughness was done using the equation proposed by Anstis[40]

$$K_{IC} = 0.016 \cdot \left(\frac{E}{H}\right)^{1/2} \cdot \frac{P}{c^{3/2}} \qquad (2)$$

Where E is the Young's modulus of the material, H is the hardness of the material, P is the indentation load, and c is the indentation crack length. Radial crack lengths were measured using a standard optical microscope. The elastic modulus was determined by

nanoindentation on polished test specimens (MML Cabinet, Berkovich tip).

Results and Discussion

Characterization of the as received alumina powder

SEM micrographs of the alumina powder used for the slip casting process are shown in Fig.1. The powder comprises irregular shaped particles of mean size about 500 nm. Moreover, it can be seen that individual particles within the powder tend to form micrometer sized agglomerates. The X-ray diffraction pattern of the alumina powder is shown in Figure 2a. The XRD pattern indicates that the powder is pure α-Al_2O_3 (corundum), and that the (104) diffraction peak is the most intense in the XRD spectrum.

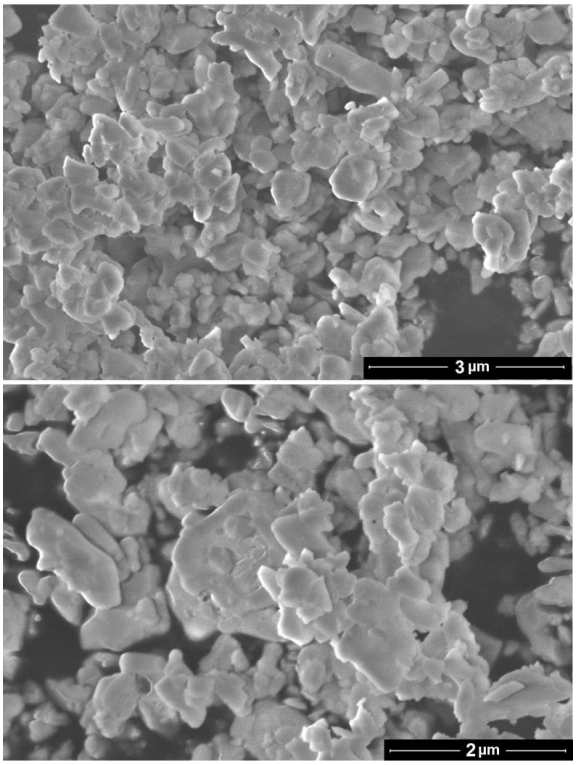

Fig. 1. Secondary electron SEM micrographs of the alumina powder used for the slip casting –pressureless sintering process.

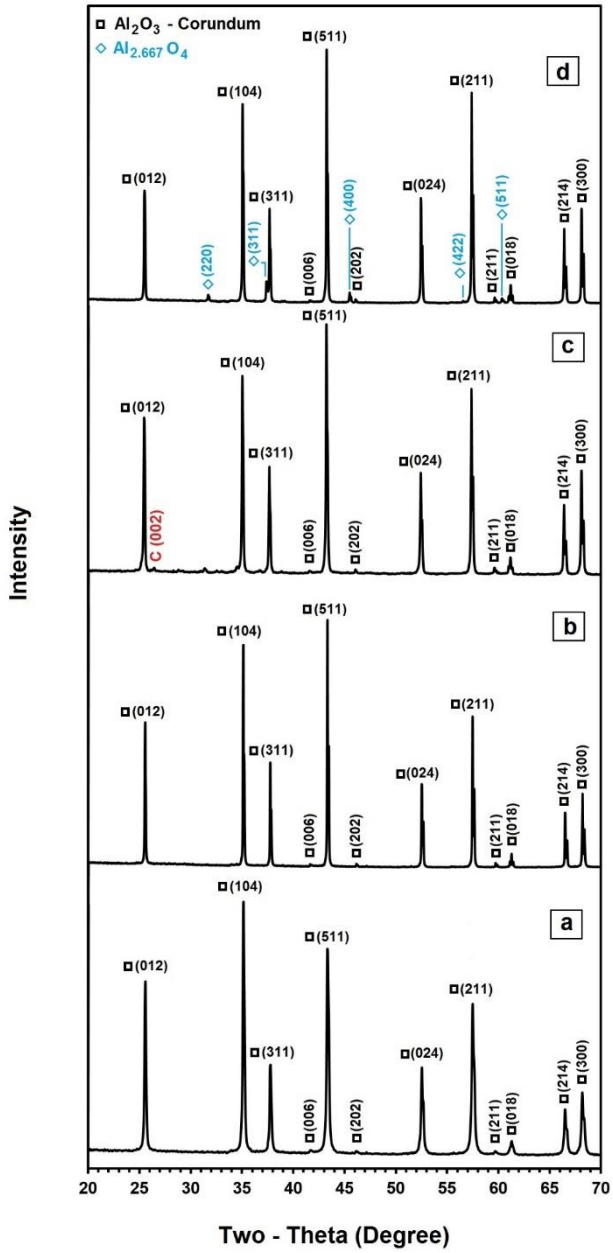

Fig.2 X-ray diffraction patterns of (a) alumina powder used for the fabrication of ceramics, and those of ceramics prepared using (b) no additive as well as (c) 1wt% graphite powder and (d) 1wt% molten salt produced graphene. The lack of appearance of (002) carbon peak in alumina-graphene spectrum is due to the low dimensionality of the graphene material in the direction perpendicular to the c-axis, and also its low relative quantity.

Molten salt preparation of graphene

Molten salt assisted electrochemical exfoliation of graphite is based on the high temperature intercalation of hydrogen into the interlayer space of graphite crystallites. In order to prepare graphene, a graphite electrode was cathodically polarized in molten LiCl, containing hydrogen cations, to deliver a constant current of 32 A, corresponding an initial cathode current density of about 1 A cm^{-2}. During the process, the space above the molten salt was purged with a stream of argon - 5% hydrogen gas, with a flow rate

of 200 mL min^{-1}, leading to the formation of hydrogen cations in molten LiCl, which is known to be able to dissolve hydrogen in the form of protons (hydrogen cations).[11,41,42]

Hydrogen cations formed are then discharged on the cathode to form hydrogen atoms, which subsequently intercalate into the interlayer space of the graphite electrode lattice. The combination of hydrogen atoms in the space between graphene layers of the graphite leads to the formation of hydrogen molecules with enough kinetic energy to overcome the Van der Waals forces between the graphene layers. Fig. 3a shows a schematic representation of the electrochemical exfoliation of graphite in molten salts. The graphite cathode is gradually eroded because of its surface exfoliation, leading to the release of graphene nanosheets into the molten salt. Fig. 3b (upper panel) shows the photograph of graphite electrode at the different stages of the process. The graphene nanosheets produced can then be retrieved from the solidified salt by water washing and filtration. Fig. 3b (down panel) exhibits the graphene nanosheets stored in glass jars during drying in an oven. It should be mentioned that the erosion of graphite cathodes in molten LiCl in the absence of hydrogen at both laboratory[43]- and bench[44]-scales has been reported in the literature, and is known to cause the formation of multi-walled carbon nanotubes and nanoparticles. In this case, it was proposed that lithium from molten salt deposits on and then intercalates into the graphite lattice, under the influence of a sufficiently negative electrode potential, leading to the expansion of the lattice. By increasing the amount of intercalated lithium, thereby enhancing the stress, the graphite lattice fragments, leading to the formation of various carbon nanoparticles and nanotubes.[45] The formation of graphene reported in this paper is, therefore, attributed to the the presence of hydrogen according to the mechanism explained above.

It is also worth mentioning that although the reduction of hydrogen cations on graphite cathodes has been investigated from a variety of electrolytes, including molten potassium bisulphate (at 245-280°C)[46] and water (at room temperature)[47], exfoliation of the graphite cathodes was not reported to occur. The exfoliating behaviour of hydrogen observed in the current paper can be explained by the high diffusion rate of hydrogen atoms into the interlayer space of the graphite lattice at 800 °C, which can be estimated[48] to be as high as 3.3×10^{-5} cm^2 s^{-1}; about 45000 and 50 times more than that at room temperature and 280°C, respectively. Therefore, the atomic hydrogen formed on the surface of the graphite cathode at 800 °C is more likely to diffuse into the graphite lattice, before combination with another hydrogen atom to form H_2 gas, thereby before escaping from the graphite surface. The combination of hydrogen atoms, therefore, has a greater chance to occur within the graphite lattice, leading to the exfoliation the graphite. It should also be considered that the pressure and particle movement and thus the kinetic energy of H_2 increases with temperature, enhancing the exfoliation process.

Fig. 4a shows the X-ray diffraction pattern of graphene nanosheets produced. The low intensity of the (002) reflection in the graphene product is indicative of its low-dimensional crystalline structure along c-axis. The Raman spectrum of the product is shown in Fig. 4b. The Raman spectrum is characterised by the presence of well defined D, G and 2D bands. In graphitic materials, D peak is caused by the defects of the graphene layers; G band is indicative of a high degree of structural ordering, and 2D-band represents the second order of the D-mode and its intensity and shape are related to the stacking order of graphene sheets along the c-axis, and the number of layers.[49]

As can be seen from Fig. 4b, the D band in the Raman spectrum of the graphene product is very weak whilst the 2D band is a sharp and symmetric peak. These features are indicative of the high quality of the graphene product. This was further confirmed by the direct SEM observations as shown in Fig.5. According to this figure, the product consists of exfoliated graphene sheets with a sheet dimension of 2–3 µm in average.

The graphene product was used in the manufacturing of alumina ceramics. In addition to graphene, commercial graphite powder and carbon nanotubes were also used for comparison.

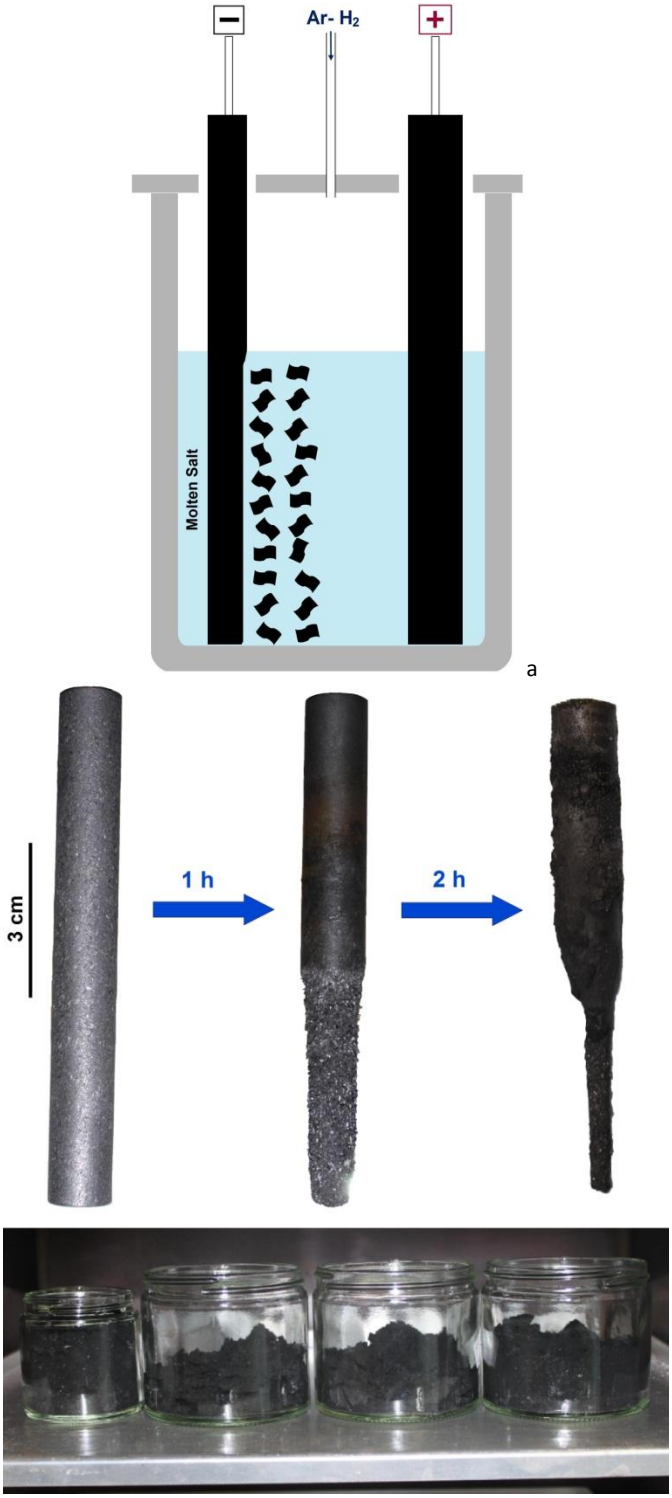

Fig. 3. (a) Schematic representation of the molten salt technique for the prepration of graphene. A cathodically polarised graphite electrode was eroded in molten LiCl containing hydrogen cations, brought about by the use of an Ar-5%H_2 flow. The eroded product, in the form of graphene nanosheets, can be retrived from the solidified salt afterward. (b) (upper panel)Photographs of the graphite electrode at different stages of the process. (down panel)The graphene nanosheets stored in glass jars during drying.

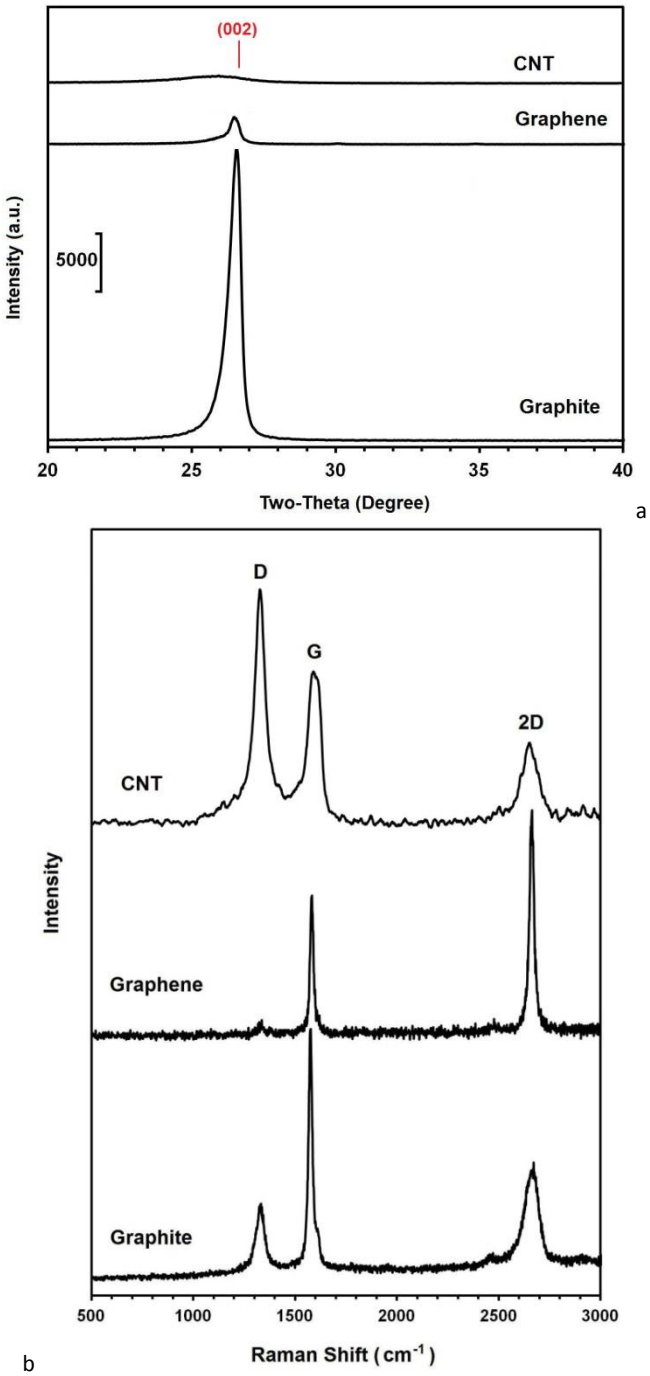

Fig.4. (a) XRD and (b) Raman spectrum of the graphite powder, graphene product and CNTs. The low intensity of C (002) XRD peak in the graphene material and CNT is due to the low dimensionality and poor crystallinity of these carbon nanostructures in the direction perpendicular to the c-axis, respectively. The D Raman band is sharper and the 2D Raman band is shorter and asymmetric in graphite powder in comparison with those of graphene, indicating that the graphite powder comprises thick stacks of graphite flakes. The results also indicate that the graphene product is of a high quality.

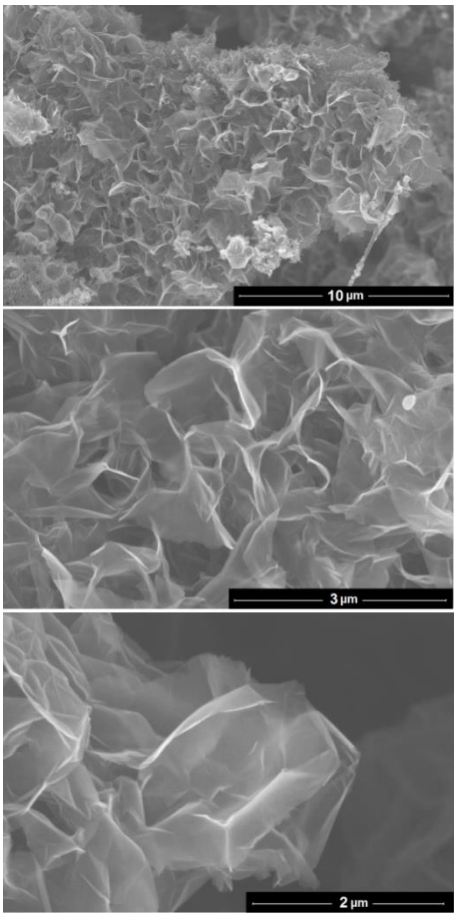

Fig.5. Secondary electron SEM micrographs showing graphene layers of the product produced by the exfoliation of graphite electrodes in molten salt. This material was used in the manufacturing of alumina ceramics.

Commercial graphite powder and carbon nanotubes

The XRD and Raman analysis of the graphite powder and CNTs used in the manufacturing of alumina ceramics are shown in Fig. 4. The relatively sharp (002) peak in the XRD pattern of the graphite powder demonstrate the abundance of graphite flakes. All the three Raman bands of graphite can be identified in the Raman spectrum of the graphite powder. As can be seen, the 2D band in the spectrum is broad and asymmetric which further confirms the existence of many-layer graphite flakes. The SEM micrograph of the graphite powder is shown in Fig. 6. As can be depicted, the material contains of randomly oriented graphite grains of several micrometers in size.

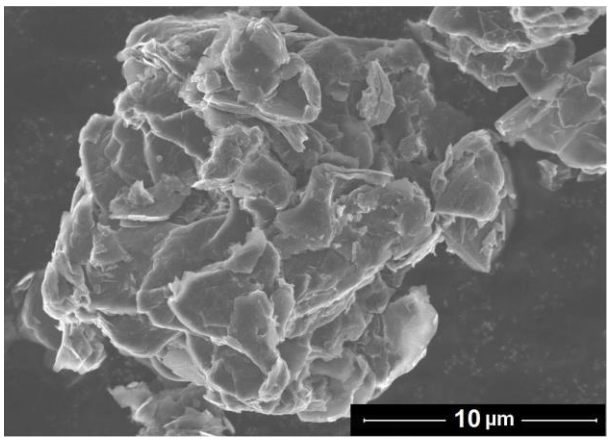

Fig. 6. Secondary electron SEM micrograph of the graphite powder used in the manufacturing of alumina-graphite ceramic.

According to Fig.4a, the (002) reflection in CNTs is weak and broadened and also shifted to lower angles compared to those recorded for the graphite powder and graphene product. This result, together with the presence of an intense D band in the Raman spectrum of CNTs (displayed in Fig. 4b) is attributed to the low crystallinity of CNTs. Secondary electron SEM micrographs of the CNTs, presented in Fig. 7, shows that the individual tubes tend to agglomerate and form large clusters up to several tens of micrometers in size.

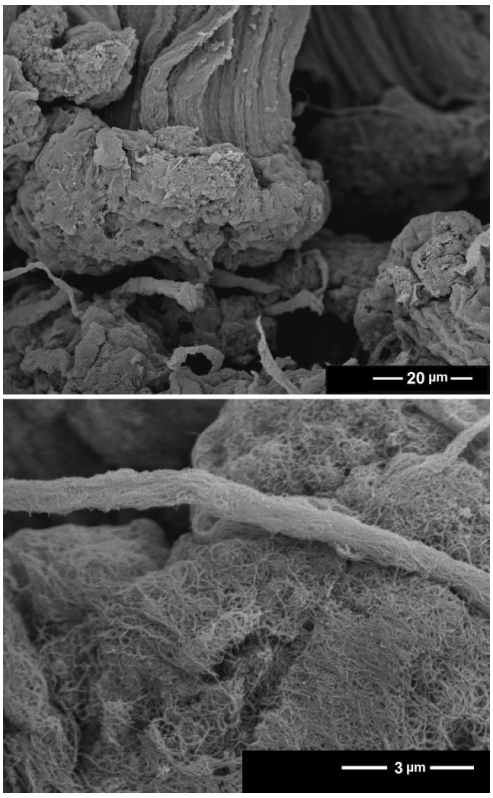

Fig. 7. Secondary electron SEM micrographs of the CNTs used in the manufacturing of alumina-graphite composites.

Preparation of alumina ceramics

The conventional low- cost slip casting process followed by pressureless sintering was used to fabricate alumina matrix ceramics by employing the molten salt-produced graphene, graphite powder, and CNTs in the fabrication process. Homogeneous slips could successfully be made for all the three carbon materials. The slip-casted green bodies were then dried and sintered at 1650°C.

It should be mentioned that slip casting process is a unique and cost effective technique for producing green bodies, in which the suspension is easily added to a permeable mould determining the shape of the object, as can be seen in Fig. 8. This manufacturing technique doesn't require expensive equipment, and is capable of producing from one to hundreds of articles.

Despite the success of producing homogeneous suspensions using all the carbon materials, on sintering, however, the CNTs failed to remain dispersed, and instead, concentrated in the centre of the sample, as shown in Fig. 9. This has been put down to the high affinity of tubes for other tubes and weak alumina-nanotube bonding. Fig. 9 also shows the X-ray diffraction analysis of the two distinctive parts of the sample's cross section. The XRD pattern of the area closer to the edge of the cross section can be indexed to the diffraction of α-Al_2O_3. The XRD pattern obtained on the centre of the sample, however, reveals extra diffraction peaks, in addition to those of α-Al_2O_3. These diffraction peaks can be indexed to $Al_{2.667}O_4$ reflections. Considering the fact that this area contains CNTs, the formation of $Al_{2.667}O_4$, with slightly lower value of O:Al atomic ratio in comparison with Al_2O_3, can be attributed to the surface reduction of Al_2O_3 by CNTs occurred during the sintering process. We will discuss it later in this paper.

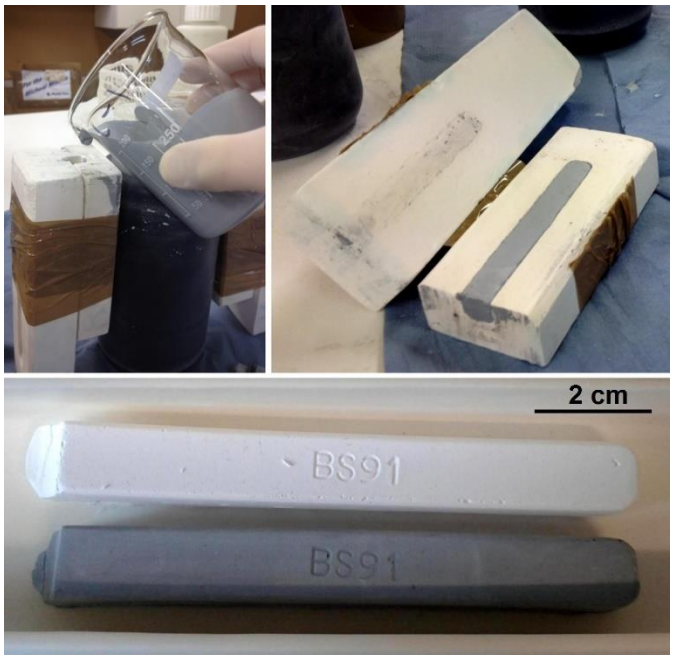

Fig.8. The slip casting process was adopted to prepare alumina and alumina-carbon green bodies. The process includes the preparation of slips of the desired amount of alumina and carbon followed by casting of the slip into a two-piece plaster mold forming rectangular specimens on loss of the water.

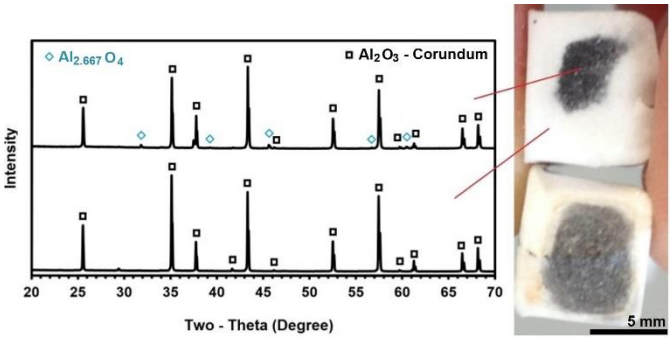

Fig. 9. Cross-section of the sintered alumina-CNT sample. CNTs failed to remain dispersed during the sintering process and concentrated in the centre of the sample. The X-ray diffraction patterns of the two distinctive parts of the cross-section are also presented.

Unlike CNTs, graphene and graphite remained mostly homogeneous on sintering, which can be attributed to the fact that graphene and graphite flakes have more difficulty in diffusing through the alumina body during the sintering process in comparison with CNTs. This is in part thanks to their wide and flat shape, but also due to their larger contact area generating stronger bonding to the alumina.

The fracture surfaces of the sintered samples are shown in Figs. 10,11 and 12, and their properties in Table 1. As it can be seen from Fig. 9(a), sintering of alumina sample led to form a coarse-grained body with a grain size of 10-20µm. The fracture toughness of the sample was measured to be 4.5 MPa $m^{1/2}$ which is in agreement with that of pressureless sintered alumina ceramics reported in the literature.[29] From Fig. 10(b), no clear change in alumina grains size could be observed by adding 1wt% graphite, although graphite flakes were well dispersed in between Al_2O_3 particles. The fracture toughness of this sample (4.31 MPa $m^{1/2}$) was slightly lower than that of alumina. It was because graphite flakes function as defects, hence lower the toughness of the material. Fig. 10(c) shows the morphology of the sample fabricated by sintering the green body containing 1wt% graphene. Surprisingly, although no visible sign of the presence of graphene could be observed; the grain sizes (2-3 µm) were much smaller than that of alumina. Furthermore, the fracture toughness of the sample had an impressive value of 6.53 MPa $m^{1/2}$. Fig. 10(c) (down panel) shows an intergranular crack propagation observed in the sample. The reason why graphene nanosheets could not be observed by SEM is probably because the graphene sheets partially covered alumina particles. It can also explain the fine grain sizes observed in the graphene containing sample. The results obtained demonstrate the obvious microstructural refining effect of molten salt produced graphene nanosheets.

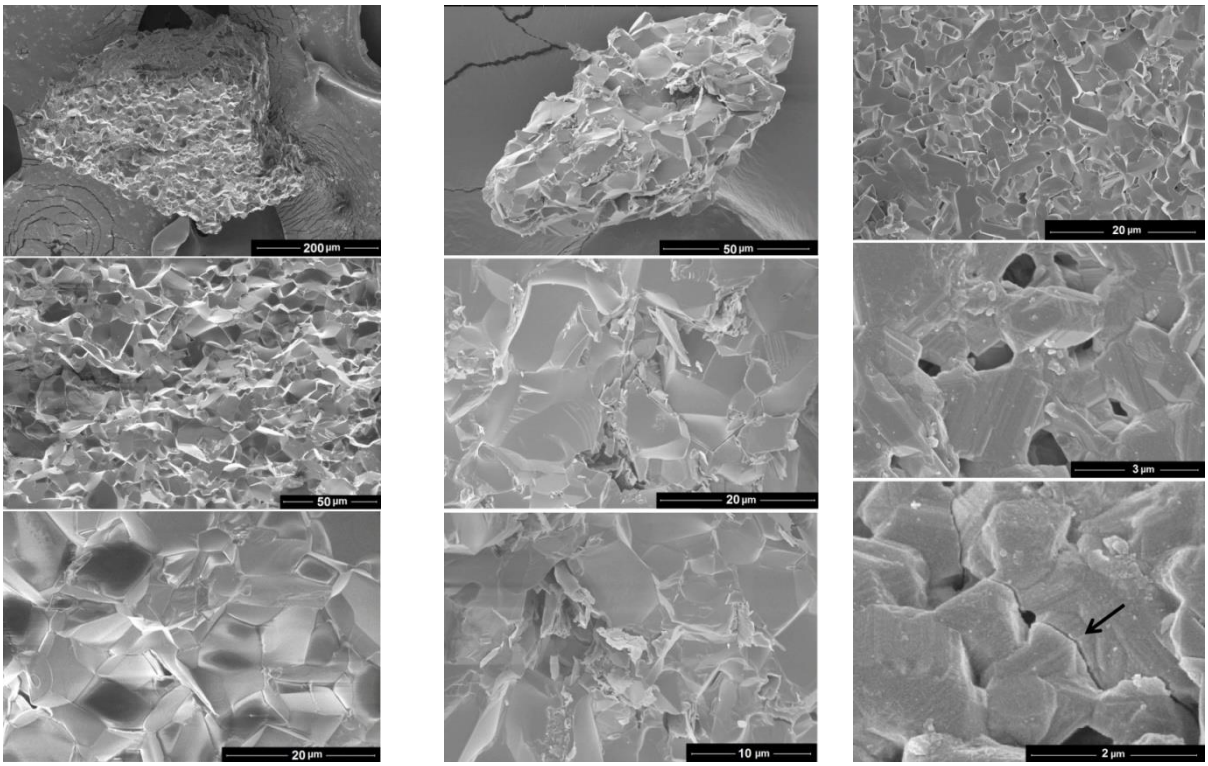

a b c

Fig. 10. Secondary electron SEM micrographs of sintered samples produced using (a) alumina, (b) alumina-1 wt%graphite, and (c) alumina-1wt% graphene. The arrow shows an intergranular crack propagation in the fine-grain microstructure.

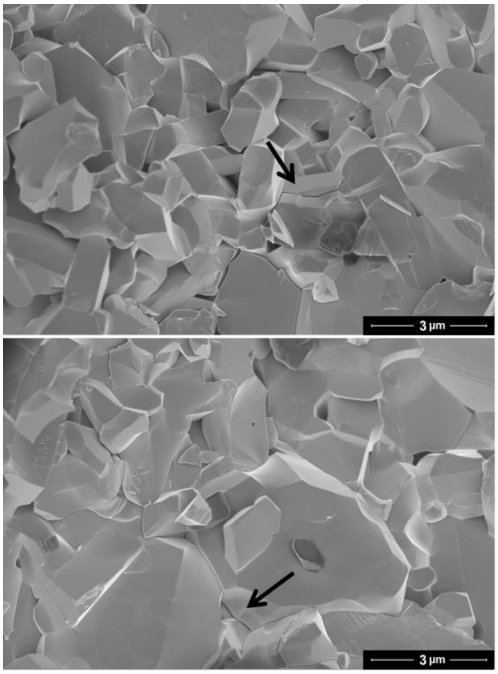

Fig. 11. Secondary electron SEM micrographs of sintered sample produced using 2wt% graphene. The arrows show intergranular crack propagation observed in the sample.

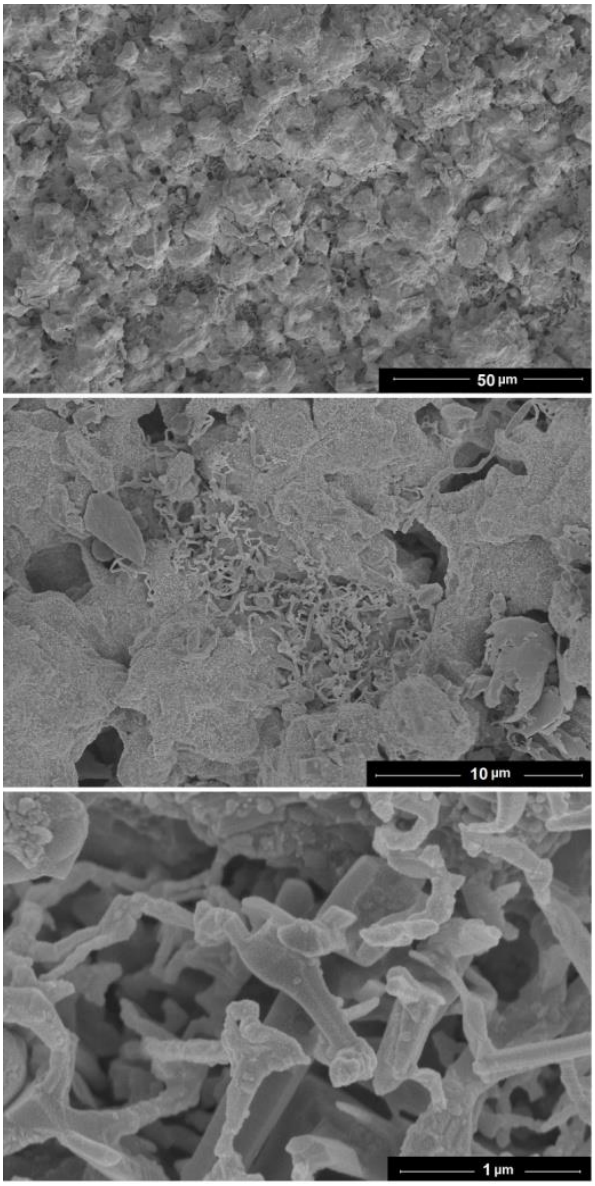

Fig. 12. Secondary electron SEM micrographs of the sintered sample produced using 0.5wt% graphene. The microsturure obtained is unique in the sense that micrometer-sized alumina particles are separated by alumina nanorods of 50-200 nm in diameter. This material exhibited an impressive fracture toughness of 6.98 MPa $m^{1/2}$, owing to its interesting morphology. Moreover, the alumina article produced is porous that makes it attractive for biomedical applications.

It is worthy to mention that microstructal changes during the heat treatment of alumina powders can be classified as coarsening and densification.[50] It is known that grain boundary and volume diffusion contributes to the densification of compacts, whilst surface diffusion is the dominant coarsening mechanism during the sintering process.[51] The presence of graphene layers around the alumina particles, during the sintering process, could reduce the surface diffusion and hence the microstructural coarsening, to some extent, is avoided. It should be noticed that the effect of graphene on toughening of alumina matrix composites depends on the method used for the fabrication of the composite. It also strongly depends on the properties of graphene used, which in turn depends on its fabrication process. For composites prepared by means of spark plasma sintering, different values of fracture toughness 3.5, 4.5 and 5.2 MPa $m^{1/2}$ have been achieved using graphene materials fabricated by liquid phase exfoliation,[37] thermal expansion/exfoliation of intercalated graphite[38] and modified Hummers method followed by hydrazine reduction.[36] The high fracture toughness obtained in the molten salt produced graphene-alumina composite can be attributed to the high flexibility of molten salt produced graphene nanosheets which enables them to be tightly folded on alumina particles reducing crack growth rate in the composite product.

In order to elucidate the effect of graphene content on the morphology and toughness of the alumina ceramic, two more composite green bodies with the graphene content of 2 and 0.5wt% were also prepared by the same method of slip casting and pressureless sintering. Figs. 11 and 12 show the SEM micrographs from the fracture surfaces of the samples, respectively. The SEM morphology of the sample fabricated using 2wt% graphene (Fig. 11) can be characterised by the presence of alumina grains having dimensions less than 5µm. The sample showed a fracture toughness of 6.40. However, and interestingly, the morphology of the sample fabricated using 0.5wt% graphene is distinctive from all other samples, consisting of alumina particles of about 6 µm which are connected to each other by alumina nanorods of 50-200nm, according to Fig. 12. The fracture toughness of this sample was measured to be 6.98 MPa $m^{1/2}$. The high toughness of this sample can be attributed to its unique microstructure in which alumina grains are separated by alumina nanorods, reducing the likelihood of grain-boundary crack propagation. The evolution of this microstructure will be explained shortly in this paper.

Table 1. Properties of alumina bodies fabricated by pressureless sintering method.

Sample	Bulk Density (g cm^{-1})	k_{IC} (MPa $m^{1/2}$)	Hv (GPa)	Reference
Al_2O_3	3.79	4.50 ± 0.60	20.3 ± 3.8	current study
Al_2O_3 + 1 wt% graphite	3.72	4.31 ± 0.24	9.8 ± 4.5	
Al_2O_3 + 0.5 wt% graphene	3.58	6.98 ±0.54	19.3 ± 4.9	
Al_2O_3 + 1 wt% graphene	3.65	6.53 ± 0.65	13.6 ± 3.6	
Al_2O_3 + 2 wt% graphene	3.63	6.40 ± 0.01	10.6 ± 0.5	
Al_2O_3-0.1 wt% CNTs	-	5.3-5.7	15.1-16.3	[55]
Al_2O_3	-	2.8	19	[56]
Al_2O_3-(0.8-1.5)vol.% graphene plates	-	3.6-4.5	18-18.5	[56]
Al_2O_3-1 vol%SiC	-	4-5	16.4	[28]
Al_2O_3	-	2.7-3.6	15.1	[28]

X-ray diffraction parents of the samples prepared by sintering of alumina, alumina-1wt% graphite, as well as alumina-1wt%graphene are shown in Fig.2. From this figure, the pure alumina sample can be identified to be fully α-Al_2O_3 (corundum). The peaks in the XRD pattern of the alumina-1wt% graphite sample can also be perfectly indexed to α-Al_2O_3. Furthermore, the (002) reflection of graphite can be clearly seen at 2h = 26.44°, no other XRD peaks could be detected. The XRD result obtained is in agreement with the SEM micrographs of Fig. 10b, where the presence of graphite flakes between alumina grains is visually confirmed. The XRD pattern of the alumina-1wt%graphene sample is shown in Fig. 2d. The XRD reflections of α-Al_2O_3 can be easily indentified in the pattern. No XRD peak corresponding to (002) reflection of hexagonal graphite structure could be observed at 2θ=26-27°. Moreover, the presence of weak reflections corresponding to $Al_{2.667}O_4$ is evident from the pattern. The similar XRD result was observed when CNTs were used in the manufacturing of alumina samples (Fig. 9). Likewise, The XRD patterns of the samples with the initial concentration of 0.5 and 2wt% graphene could also be characterised by the presence of α-Al_2O_3 as the major phase with a minute amount of $Al_{2.667}O_4$ (the diffraction patterns are not shown here). This result is interesting and demonstrates that, unlike graphite flakes, CNTs and graphene have a reducing effect against Al_2O_3, leading the formation of oxygen vacancies on the Al_2O_3 surface. It should be mentioned that α-Al_2O_3 with oxygen vacancy has been prepared so far only by complicated techniques such as energetic heavy ions bombardment[52] and aluminium vapour treatment[53] of α-Al_2O_3. Formation of the alumina nanorodes, as observed in Fig.11, can

be attributed to the solid phase directional growth of α-Al_2O_3 with oxygen vacancies occurred during sintering. The surface reduction of Al_2O_3 into $Al_{2.667}O_4$ with lower oxygen content provides a chemical driving force for surface diffusion and subsequent crystal growth of aluminium oxide into the one dimensional nanostructure. Similar solid state growth influenced by surface oxygen vacancies has also been observed for SnO_2.[54] Owing to their unique microstructure and mechanical properties, the resulting alumina articles fabricated using molten salt produced graphene, can be considered for applications such as biomedical and dental implants where the fracture toughness of alumina article is critical.

The results obtained in this paper indicate that molten salt produced graphene can be employed to enhance the mechanical properties of alumina ceramics manufactured by the conventional slip casting and pressureless sintering method. These results are of specific importance for technical application, considering the scalability and economic feasibility of the molten salt process. This process consumes mainly graphite, H_2 and electricity. A part of the salt used evaporates from the crucible, due to the high operating temperature of about 800°C, and deposits on the cooler inner surface of the inconel retort. Apart from this, the consumption of LiCl is small supporting the idea that the process mainly proceeds by the cathodic discharge of H^+ and not Li^+. At the end of the process, a mixture of graphene and solidified sold is obtained. The salt is highly soluble in water, enabling one to separate LiCl solution and graphene using vacuum filtration. Lithium chloride can then be retrieved from the solution by a simple water evaporation method. Moreover, the Cl_2 gas evolved on the anode, during the electrochemical process, reacts with H_2 available in the atmosphere above the molten salt, and the HCl produced mostly dissolves into the melt providing hydrogen cations. The production rate of graphene by this method is estimated to be 450 g graphene per litre of molten salt per day. The process uses graphite electrodes which are readily available with diameters as large as 80 cm at a low price of about US $4000 per metric tons. The specific energy consumption and the cost of producing high quality graphene can be estimated to be about 25 kWh kg^{-1} and US $10–20 kg^{-1}, respectively. The economic production in large quantities of high quality graphene in molten salts is the driving force for its evaluation in various applications.

Conclusions

High quality graphene nanoheets were prepared by the exfoliation of graphite in molten salt. The graphene product along with graphite powder and CVD-produced CNTs were used as additive in the fabrication of alumina articles using the convenient method of slip casting and pressureless sintering. Graphene was shown to outperform other carbon additives to increase the mechanical properties of pressureless sintered alumina. Addition of 0.5wt% graphene led to the formation of a microstructure consisting of micrometer sized alumina particles separated by networks of alumina rods exhibiting a superior toughness of 6.98 MPa $m^{1/2}$, hardness of 19.3 GPa and flexural strength of 368 MPa. The formation of alumina nanorods during the sintering process was assigned to the directional growth of alumina crystallites influenced by the surface oxygen vacancies.

Acknowledgements

The Worshipful Company of Armourers and Brasiers is thanked for funding support for this research. Technical contributation from Mr M. Misson (Almath Crucibles Ltd) is greatly appreciated.

1 G.Z. Chen, D.J. Fray and T.W. Farthing, *Nature*, 2000,**407**,361.
2 R. Abdulaziz, L. D. Brown, D. Inman, S. Simons, P. R. Shearing and D. J.L. Brett, *Electrochem. Commun.*, 2014, **41**, 44.
3 Y. Sakamura, M. Iizuka, S. Kitawaki, A. Nakayoshi and H. Kofuji, *J. Nucl. Mater.*,2015, **466**, 269.
4 J.M. Hur, S.S. Hong and H. Lee, *J. Radioanal. Nucl. Ch.*, 2013, **295**, 851.
5 B.Jackson, M. Jackson, D. Dye, D. Inman and R.Dashwood, *J. Electrochem. Soc.*, 2008,**155**, E171-E177.
6 M. Gaune-Escard and K. R. Seddon (Ed),Molten Salts and Ionic Liquids: Never the Twain? D. D. Jayaseelan, Z. LI, W. Edward Lee, S. Zhang, Molten Salt Synthesis of Ceramic Materials, *Wiley*, 2012.
7 A.R. Kamali and D.J. Fray, *Ceram. Intern*. 2014,**40**, 1835.
8 W. K. Hsu, J. P. Hare, M. Terrones, H. W. Kroto, D. R. M. Walton and P. J. F. Harris, *Nature*,1995, **377**, 687.
9 A.R. Kamali and D.J. Fray, *Chem. Commun.*,2015, **51**, 5594.
10 A.R.Kamali and D.J.Fray, *Carbon*, 2013,**56**, 121.
11 A.R.Kamali and D.J.Fray, *Nanoscale*, 2015, **7**, 11310-11320.
12 L. Hou, L. Lian, D. Li, G. Pang, J. Li, X. Zhang, S. Xiong and C. Yuan, *Carbon*, 2013, **64**, 149.
13 B. Jia and L. Zou, *Carbon*, 2012, **50**, 2315.
14 A. R. Kamali and D. J. Fray, *J. New Mater. Electrochem. Syst*., 2010, **13**, 147.
15 G. Wang, X. Shen, J. Yao and J. Park, *Carbon*, 2009, **47**, 2049.
16 H. Wu, H. Li, G. Sun, S. Ma and X. Yang, *J. Mater. Chem. C*, 2015, **3**, 5457.
17 T. Kuilla, S. Bhadra, D. Yao, N. H. Kim, S. Bose and J. H. Lee, *Prog. Polym. Sci*., 2010, **35**, 1350.
18 H. Porwal, S. Grasso and M. J. Reece, *Adv. Appl. Ceram*., 2013, **112**, 443.
19 R. Raccichini,A. Varzi,S. Passerini and B. Scrosati, *Nature Mater.,2015,***14**,271.
20 V. Nicolosi, M. Chhowalla, M. G. Kanatzidis, M. S. Strano and J. N. Coleman, *Science*, 2013, **340**, 1226419.
21 J. S. Bunch, Y. Yaish, M. Brink, K. Bolotin and P. L. McEuen, *Nano Lett*., 2005, **5**, 287.

22 K. S. Kim, Y. Zhao, H. Jang, S. Y. Lee, J. M. Kim, K. S. Kim, J. H. Ahn, P. Kim, I. Y. Choi and B. H. Hong, *Nature*, 2009, **457**, 706.
23 P.Boch, J.C.Niepce, Ceramic Materials:Processses, Properties and Applications,*ISTE Ltd*,UK, 2007.
24 R.B.Heimann, Classic and Advanced Ceramics:From Fundamentals to Applications, *Wiley-VCH*, 2010.
25 M. Øiloa and G.e D. Quinn, *J. Mech. Behav. Biomed*.,2016, 53,93.
26 T.Usami, M.Komatsu, H.Mizutani and T.Kaneda, *J. Oral Maxillofac. Surg.*,1966, **46**,507.
27 J. Chevalie and L. Gremillard, *J. Eur. Ceram. Soc.* 29 (2009) 1245–1255.
28 H. Reveron, O. Zaafrani and G. Fantozzi, *J. Eur. Ceram. Soc.,*2010, **30**,1351.
29 J.P.Auerkari, Mechanical and physical properties of engineering alumina ceramics, ulkaisija-Utgivare, Finland,1996.
30 J.Chevalier, *Biomater*. ,2006, **27**, 535.
31 Y.Q. Wu, Y.F. Zhang, G.Pezzotti and J.K. Guo, *J. Eur. Ceram Soc.*,2002, **22**,159.
32 J. Lalande, S. Scheppokat, R. Janssen and N. Claussen, *J. Eur. Ceram Soc.*, 2002,**22**,2165.
33 W. H. Tuan and R. J. Brook,The Toughening of Alumina with Nickel Inclusions, *Journal of the European Ceramic Society* 6 (1990) 31-37.
34 S.W. Kim,S.L. Cockcroft, K.A. Khalil and K. Ogi, *Mater. Sci. Eng. A*. 2010, **527**,4926.
35 P. A. Trusty and J. A. Yeomans, *J. Eur. Cerm. Soc.*, 1997,**17**, 495.
36 K. Wang, Y. Wang, Z.Fan, J. Yan and T. Wei, *Mater.Res. Bull*., 2011,**46** 315.
37 H. Porwal, P. Tatarko, S. Grasso, J. Khaliq,I.Dlouhy and M. J. Reece, *Carbon*, 2013,**64**,359.
38 J. Liu, H.Yan and K.Jiang, *Ceram. Intern*.,2013, **39**, 6215.
39 Standard Test Methods for Flexural Properties of Unreinforced and Reinforced Plastics and Electrical Insulating Materials, ASTM Standard D790-10, ASTM International, West Conshohocken, 2010.
40 G.R.Anstis, P.Chantikul, B.R.Lawn and D.B.Marshall, *Am. Ceram. Soc*.,1981, **64**,533.
41 A.R. Kamali, D.J.Fray and C Schwandt, *J. Therm.Anal.Calorim*.,2011,**104**,619.
42 A.R.Kamali, *Green Chem*., 2016, DOI: 10.1039/C5GC02455B**.**
43 G.Z. Chen, X.D. Fan, A. Luget, M.S.P. Shaffer, D.J. Fray and A.H. Windle, *J. Electroanal. Chem*.,1998, **446**, 6.
44 A. R. Kamali and D. J. Fray, *Carbon*, 2014, **77**, 835.
45 A. T. Dimitrov, G. Z. Chen, I. A. Kinloch and D. J. Fray, *Electrochim. Acta,*2002, **48**, 91.
46 E. J. Balskus, W. E. Triaca and A. J. Aria, *Electrochim.Acta*, **1972**, 17, 45.
47 P. B.Vilanova,S. Puig,, R. G.Olmos,A. V.Pons, L. Bañeras, M. D. Balaguer and J. Colprim, *Int. J. Hydrogen Energy*, 2014, **39**,1297.
48 C. P. Herrero and R. Ramirez, *J. Phys. D: Appl. Phys*., 2010, **43**,255402.
49 M. S. Dresselhaus, A. Jorio and R. Saito, *Annu. Rev.Condens. Matter. Phys.,* 2010, **89**, 108.
50 N. J. Shaw and R. J. Brook, *J. Am. Ceram. Soc*., 1986, **69** 107.
51 F. Raether and P. Schulze Horn, *J. Eur.Ceram. Soc*.,2009, **29**, 2225.
52 F. Jollet, J.P. Duraud, C. Nogera, E. Dooryhee and Y. Langevin, *Nucl. Instr. Meth. Phys. Res.*,1990, **B46**,125.
53 A. I. Surdo, V. S. Kortov , V. A. Pustovarov and V. Yu. Yakovlev, *phys. stat. sol.*,2005, **1**, 527.
54 A.R.Kamali and D.J.Fray, *Mater. Sci. Eng. B*,2012, **177**, 819.
55 M. Michalek, K. Bodisova, M.Michalkova, J.Sedlaceka and D. Galusek, *Ceram. Intern*.,2013, **39**,6543.
56 J. Liu, Y. Yang, H. Hasssinin, N. Jumbu, S. Deng, Q. Zuo, and K. Jiang, *Appl. Mater. Interfaces,* **DOI:** 10.1021/acsami.5b10424.